Coexistence of polar distortion and metallicity in $PbTi_{1-x}Nb_xO_3$

Jun-xing Gu,[1,2] Kui-juan Jin,[1,2,3,*] Chao Ma,[1,2] Qing-hua Zhang,[1,2] Lin Gu,[1,2,3] Chen Ge,[1,2] Jie-su Wang,[1,2] Can Wang,[1] Hai-zhong Guo,[1,2] and Guo-zhen Yang[1,2,3]

[1]*Beijing National Laboratory for Condensed Matter Physics, Institute of Physics, Chinese Academy of Sciences, Beijing 100190, China*

[2]*School of Physical Sciences, University of Chinese Academy of Sciences, Beijing 100190, China*

[3]*Collaborative Innovation Center of Quantum Matter, Beijing 100190, China*

(Received 13 August 2017; revised manuscript received 18 October 2017; published 31 October 2017)

Ferroelectricity has been believed unable to coexist with metallicity since the free carriers can screen the internal Coulomb interactions of dipoles. Very recently, one kind of material called *ferroelectric metal* was reexamined. Here, we report the coexistence of metallicity and polar distortion in a candidate for ferroelectric metal $PbTi_{1-x}Nb_xO_3$ via doping engineering. The ferroelectriclike polar distortion in all the doped $PbTi_{1-x}Nb_xO_3$, with x ranging from 0.04 to 0.12, was observed by the piezoresponse force microscopy and the scanning transmission electron microscopy measurements. $PbTi_{1-x}Nb_xO_3$ films become more conductive with more doping density, and a metallic behavior emerges when x reaches 0.12. Our first-principles calculations further revealed that the doped Nb ions in the films can only provide free electrons, but are not able to damage the dipoles in unit cells even with the heaviest doping density of 0.12. We believe that these results confirm a feasibility of realizing the coexistence of metallicity and polar distortion for other ferroelectrics in a common way, and motivate the synthesis of some new materials with artificially designed properties even incompatible in nature.

DOI: 10.1103/PhysRevB.96.165206

I. INTRODUCTION

Since Anderson and Blount proposed the statement of "ferroelectric metal" over five decades ago [1], this type of material has mostly stayed in conceptual or theoretical designing. Such materials should be very hard to obtain because the free carriers screen the long-range Coulomb interaction, and therefore weaken the ferroelectric polar distortion. Nevertheless, recently unambiguous experimental evidence of ferroelectriclike structure transition in metallic material $LiOsO_3$ has again attracted much attention on the metals with noncentrosymmetric structures, which were observed at low temperature below 150 K [2–8]. Yet, they remain challenging to discover [8,9]. So far no room-temperature candidate for the coexistence of polar distortion and metallicity has been obtained. Different from the noncentrosymmetric metals, another possible route toward ferroelectric metal is looking for a ferroelectric insulator whose polar distortion survives doping of carriers. Unfortunately, based on the extensive research on the prototypical ferroelectric $BaTiO_3$ with doping engineering, it has been found that the doped electrons have weakened the polar distortion of $BaTiO_3$, or even erased the polar distortion when a critical concentration is reached [10–13]. Recently, Raghavan *et al.* pointed out that the ferroelectricity and mobile carriers can coexist in $SmTiO_3/BaTiO_3$ heterostructure by purely electrostatic doping [14]. In addition, $PbTiO_3$ is another common ferroelectric material, but not enough attention has been paid to it as a doped ferroelectric [15]. Very recently, our theoretical study revealed that $PbTiO_3$ is a wonderful candidate for the doped ferroelectric materials [16]. We have proposed that the lone-pair-driven polar distortion not only persists, but might also be enhanced with electron doping [16]. The mechanism is that, in the lone-pair ferroelectric perovskite oxides (ABO_3, A being the lone-pair cation), the doped electrons do not considerably impact the $A-O$ or $B-O$ covalence bonds that are responsible for the polar distortions [17].

Here we present a coexistence of polar distortion and metallicity in Nb-doped $PbTiO_3$ at room temperature. In this work, we fabricated the $PbTi_{1-x}Nb_xO_3$ (PTNO) films with various doping concentrations ($x = 0.04$, 0.06, 0.08, and 0.12) on (001)-oriented $SrTi_{0.993}Nb_{0.007}O_3$ (STNO) conductive single-crystal substrates. The piezoresponse loops were observed by piezoresponse force microscopy (PFM) in films with all above doping densities, in spite of the large leakage currents in the highly doped samples. To confirm the ferroelectricity or, more accurately, the existence of the noncentrosymmetric structure of the PTNO films, a distinct off-centering of the Ti ion was directly characterized by scanning transmission electron microscopy (STEM). Then macroscopic ferroelectric hysteresis loops (P-E loops) measurements show that the polarization induced by Ti ion displacements cannot be totally screened by the doped electrons. With increasing x, the temperature-dependent behavior of the PTNO films changes from insulating to semiconducting, and further to the metallic. Our first-principles calculation further shows that the electron from the doped Nb mainly locates around one of the four nearest Ti ions to Nb and behave itinerantly. Those doped electrons allow the $PbTi_{0.88}Nb_{0.12}O_3$ to present the metal-like behavior, whereas they are not able to effectively impact the covalence bonds of Pb–O and those of Ti–O, so that they cannot damage the polar distortions nor the individual dipole in each unit cell. We believe that the present work not only realizes a room-temperature candidate with the coexistence of polar distortion and metallicity, but also paves the way for doping some ferroelectrics for broadening the class of ferroelectric metals, which has very few candidates so far, but with very unusual properties such as unconventional optical responses [18,19], magnetoelectricity [20], and superconductivity [21,22].

*Corresponding author: kjjin@iphy.ac.cn

II. METHODS

A. Experimental

The PTNO films with $x = 0.04$, 0.06, 0.08, and 0.12 were epitaxially deposited on (001)-oriented STNO conductive single-crystal substrates by laser molecular-beam epitaxy. The conductive layer acts as a bottom electrode in the hysteresis test. During the deposition, we use the commercial $PbTi_{1-x}Nb_xO_3$ ceramic target materials with $x = 0.04$, 0.06, 0.08, and 0.12. Therefore, the sample stoichiometric proportion should be nearly equal to the target materials. A XeCl 308-nm excimer laser was used with an energy density of 1.5 J cm^{-2} and a repetition rate of 2 Hz. During the deposition, the oxygen pressure was approximately 40 mTorr, and the temperature of substrates was 520 °C. The thicknesses of the $PbTi_{1-x}Nb_xO_3$ (PTNO) films are around 200 nm. After the deposition, the samples were *in situ* annealed at 520 °C for 20 min, and then cooled down to room temperature.

The atom-substituted doping and the crystal structures were identified by x-ray absorption spectroscopy (XAS) and the conventional θ-2θ x-ray diffraction (XRD) method, respectively. The ferroelectric domain structure and local piezoresponse-voltage relationship were characterized by the measurement of PFM in dual ac resonance tracking mode [23]. Temperature-dependent resistivity was measured by the combination of a temperature controller (Linkam Scientific Instrument) and a semiconductor parameter analyzer (Keithley 4200) to determine the conductive behavior. For electrical measurements, circular Au electrodes with 100-μm diameter were deposited on the surface of the PTNO/STNO. The ferroelectric hysteresis loops were measured by a ferroelectric test system (Radiant Technologies) to quantitatively evaluate the remnant polarization. Finally, we visualize the polarization of ionic displacement at the atomic scale by using the aberration-corrected high-angle annular dark-field (HAADF) Z-contrast STEM imaging.

B. Theoretical

For simplicity, 0.125 doping concentration instead of 0.12 doping concentration is investigated by constructing a $2 \times 2 \times 2$ supercell of $PbTiO_3$ and substituting one Ti by Nb. Density-functional theory (DFT) calculations are performed within the generalized gradient approximation on the basis of the projector augmented wave [24] method as implemented in the Vienna *ab initio* simulation package (VASP) [25]. The exchange and correlation functional parametrized by Perdew-Becke-Ernzerhof [26] is adopted. The electronic configurations of involved atoms are as follows: Pb ($5d^{10}6s^26p^2$), Nb ($4s^24p^64d^45s^1$), Ti ($2s^22p^63d^24s^2$), and O ($2s^22p^4$). An effective Hubbard term $U_{\text{eff}} = U - \text{J}$ using Dudarev's approach [27] is included to treat the Ti $3d$ orbital, and $U_{\text{eff}} = 3.27$ eV generates the most suitable structure compared to the experimental structure. A 520-eV energy cutoff of plane-wave basis set is taken for all calculations. For structure optimizations, atomic positions are relaxed until the energy differences are within 1×10^{-7} eV and all forces are smaller than 0.5 meV Å^{-1}.

III. RESULTS AND DISCUSSION

In the PTNO films, tetravalent Ti atoms are partly substituted by pentavalent Nb atoms. Due to the similar sizes between Nb^{5+} ($r = 0.64$ Å) and Ti^{4+} ($r = 0.61$ Å) ions, substitution of Ti by Nb does not introduce much disorder or lattice distortion in the primary $PbTiO_3$ tetragonal structure [28]. The θ-2θ XRD and XAS confirm this Ti^{4+} substitution in our fabricated PTNO films rather than the formation of new compounds (see Supplemental Material, Fig. S1 [29]) [30]. To investigate the ferroelectricity of the PTNO films, ferroelectric domains were characterized by PFM. Figures 1(a)–1(d) show the out-of-plane PFM phase images, and Figs. 1(e)–1(h) show the corresponding local piezoresponse phase-voltage loops. For the piezoresponse phase-voltage loops, the piezoresponse phases were recorded while the voltage was off. The corresponding out-of-plane PFM amplitude images and topography images are given in Supplemental Material, Figs. S2(a)–S2(h) [29]. When ac voltage is applied to the surface of a ferroelectric by a conductive tip of PFM, converse piezoelectric effect can induce a resonance of the sample surface, and then the resonance amplitude and phase can be detected by the tip [23]. The change of the resonance phase implies that the polarization changes from one direction to another. Therefore, the areas with different piezoresponse phase can exhibit the different ferroelectric domains. As shown in Fig. 1(a), strip domains were detected on the surface of the $PbTi_{0.96}Nb_{0.04}O_3$. Little relevance between the phase image and the topography image [as shown in Supplemental Material, Fig. S2(a) [29]) can eliminate the interference from topographic artifacts. In addition, the local piezoresponse phase-voltage loop in Fig. 1(e) has two well-defined states with 180° phase difference. We can conclude that the $PbTi_{0.96}Nb_{0.04}O_3$ sample shows a good ferroelectricity in common with the mother compound $PbTiO_3$. For the samples with increasing concentration of Nb, the $PbTi_{0.94}Nb_{0.06}O_3$ also has a distinguishable domain structure in the PFM phase image [Fig. 1(b)] and has 180° phase difference in the local piezoresponse loop [Fig. 1(f)]. However, $PbTi_{0.92}Nb_{0.08}O_3$ and $PbTi_{0.88}Nb_{0.12}O_3$ do not exhibit the same property as those with x less than 0.08. As shown in Figs. 1(c) and 1(d), the domain structure is amorphous for the $PbTi_{0.92}Nb_{0.08}O_3$ and is even undetectable for the $PbTi_{0.88}Nb_{0.12}O_3$. We believe that the inevitable leakage currents are responsible for the poor PFM images in the heavily doped films. Leakage currents could weaken the electric field applied on the sample, and further affect the piezoresponse signal which was read by PFM. It is also worth pointing out that the "leakage current" is used for describing current in dielectrics. However, it can be seen from this paper that the Nb doping transformed the PNTO into conductive material. In fact, we have observed the local piezoresponse loops in the $PbTi_{0.92}Nb_{0.08}O_3$ and the $PbTi_{0.88}Nb_{0.12}O_3$ films, even with much noise as shown in Figs. 1(g) and 1(h), respectively. In order to further illustrate the ferroelectric properties of the four kinds of Nb-doped $PbTiO_3$ samples, we have written two nested square domains by applying -25 V bias on the central square and $+25$ V bias on the outside part on a $3\ \mu\text{m} \times 3\ \mu\text{m}$ area of each sample. Figures 1(i)–1(l), respectively, show the out-of-plane PFM phase images of these areas on the surfaces

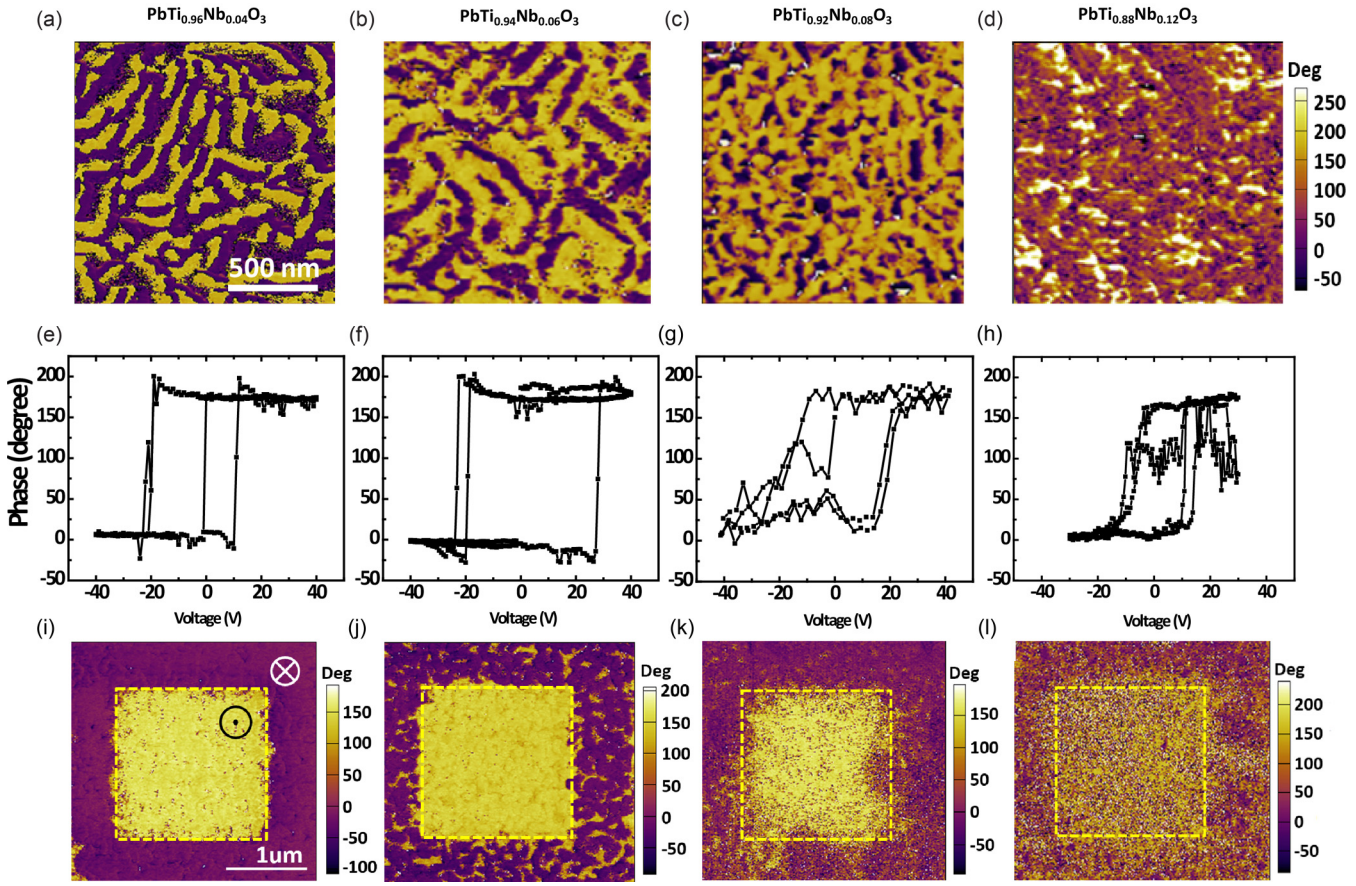

FIG. 1. Out-of-plane PFM phase images of the (a) $PbTi_{0.96}Nb_{0.04}O_3$, (b) $PbTi_{0.94}Nb_{0.06}O_3$, (c) $PbTi_{0.92}Nb_{0.08}O_3$, and (d) $PbTi_{0.88}Nb_{0.12}O_3$ films. Corresponding local piezoresponse phase-voltage loops for the (e) $PbTi_{0.96}Nb_{0.04}O_3$, (f) $PbTi_{0.94}Nb_{0.06}O_3$, (g) $PbTi_{0.92}Nb_{0.08}O_3$, and (h) $PbTi_{0.88}Nb_{0.12}O_3$ films. Out-of-plane PFM phase images of nested square domains with opposite polarization directions written using an AFM tip with ±25 V bias on the surfaces of the (i) $PbTi_{0.96}Nb_{0.04}O_3$, (j) $PbTi_{0.94}Nb_{0.06}O_3$, (k) $PbTi_{0.92}Nb_{0.08}O_3$, and (l) $PbTi_{0.88}Nb_{0.12}O_3$ films.

of the $PbTi_{0.96}Nb_{0.04}O_3$, $PbTi_{0.94}Nb_{0.06}O_3$, $PbTi_{0.92}Nb_{0.08}O_3$, and $PbTi_{0.88}Nb_{0.12}O_3$ after poling by the tip. As we can see, the contrast between up and down ferroelectric domains of $PbTi_{0.96}Nb_{0.04}O_3$ is sharp; with the increase of Nb doping, the contrast became inconspicuous and the boundary of the up and down ferroelectric domains got blurred. For the conductive materials or the dielectrics with large leakage current, it is hard to define the ferroelectricity. In fact, a conductive material with a noncentrosymmetric structure already can be taken as the candidate for ferroelectric metal.

The ferroelectric polarization of $PbTiO_3$ originates from the *A*-site (Pb) lone-pair mechanism. All of the five atoms in the unit cell of $PbTiO_3$ have polar displacements to form the noncentrosymmetric structure (the $P4mm$ phase). To confirm the polar distortion coexisting with Nb doping, the atomic-scale distinguished STEM imaging was utilized. Figures 2(a) and 2(b) represent the aberration-corrected high-angle annular dark-field STEM images of the lightly doped $PbTi_{0.96}Nb_{0.04}O_3$ and the heavily doped $PbTi_{0.88}Nb_{0.12}O_3$, respectively. In the HAADF images, the intensity of atom columns is approximately proportional to Z^2, where Z is the atomic number. Therefore, the brightest dots denote the Pb columns and the weaker dots denote the Ti (Nb) columns. We determined the position of atoms by the peak of the intensity. The Ti (Nb) off-centering with respect to the nearest eight Pb atoms is used to represent the polar distortion. On the other hand, the intensity of the center atoms in Fig. 2(b) (with 0.12 Nb doped) is higher than that in Fig. 2(a) (with 0.04 Nb doped), showing the sample with more Nb doping in Fig. 2(b) rather than that in Fig. 2(a). From Figs. 2(a) and 2(b), we can observe distinct domains in both images with 180° and 90° domain walls, which is the characteristic of the pure ferroelectric $PbTiO_3$ [31]. The zoom-in STEM images of the two samples are shown in Figs. 2(c) and 2(d), respectively. Obvious displacement of Ti (Nb) ions relative to the center of mass of the four nearest Pb neighbors is marked in these two zoom-in images. For tetragonal ferroelectric $PbTiO_3$, the polarization direction is opposite to the displacement vector of center cations [31]. Based on this, upward polarization and rightward polarization are labeled in Figs. 2(c) and 2(d), respectively. More importantly, these results demonstrate that the polar distortion still exists in the heavily doped $PbTi_{0.88}Nb_{0.12}O_3$ samples. It is completely different from the well-studied doped $BaTiO_3$, in which the polar distortion was weakened or vanished by the electron doping [10–13]. In fact, the definition of ferroelectric metals evolved more broadly in the previous reports than when it first came out decades ago. As reported in Refs. [2–12], doped ferroelectrics and noncentrosymmetric metals are all supposed to be the candidates for ferroelectric metal. However, the ferroelectriclike macroscopic remnant

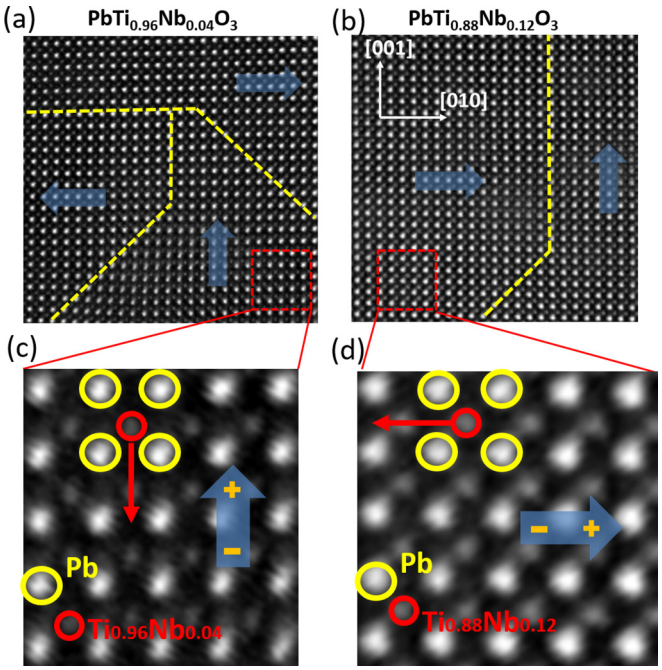

FIG. 2. HAADF-STEM images of (a) $PbTi_{0.96}Nb_{0.04}O_3$ and (b) $PbTi_{0.88}Nb_{0.12}O_3$. Yellow dashed lines highlight the domain walls. (c), (d) Zoom-in STEM images corresponding to the areas marked in (a) and (b), respectively. Red arrows denote the direction of Ti (Nb) displacement with respect to the four nearest Pb. Blue arrows denote the direction of local polarization induced by the ionic displacement.

polarization had not been measured out in any of these "ferroelectric metals" before.

In order to prove whether the polar distortion in PTNO can provide a macroscopic remnant polarization, we performed a macroscopic ferroelectricity measurement using a ferroelectric tester. Figure 3(a) shows the ferroelectric hysteresis loops (*P-E* loops) of Au/PTNO/STNO at ambient temperature. It was obtained from the remanent capacitance component, derived by subtracting one hysteresis loop from another inverse hysteresis loop. This measure mode is provided by the ferroelectric test system (Radiant Technologies) to minimize the removable charges contribution on the polarization signals. The measured frequency of the *P-E* loops was set to 10 kHz. All of these samples exhibit distinguishable *P-E* loops, in spite of that none of these loops are saturated. We believe the large leakage current is responsible for the unsaturation of *P-E* loops [32]. Even the heavily doped $PbTi_{0.88}Nb_{0.12}O_3$ has nonzero remnant polarizations when the electric field drops to zero. The *P-E* loops in the remnant polarization mode are shown in Fig. 3(b) to eliminate the contribution from leakage. Besides, we carried out the positive-up negative-down measurement to capture the remnant polarization quantitatively. For pulse delay of 1000 ms and pulse width of 1 ms, the twofold remnant polarization of $PbTi_{0.88}Nb_{0.12}O_3$ is $1.54\,\mu C/cm^2$. This numerical value is small for a traditional ferroelectric; however, it is rarely enough for a high leaky dielectric or a conductive material. This demonstrates that, more than the existence of internal polar distortion in the heavily doped $PbTi_{0.88}Nb_{0.12}O_3$ films, the polarization charges induced by the polar distortion are not completely screened out by the itinerant electrons. Therefore, it should be found out whether the dopant Nb atoms provide enough itinerant electrons to transform the conductive behavior of the PTNO films from the insulating into the metallic.

Pentavalent Nb atoms are regarded as donors which provide free electrons for the Ti^{4+} site substitution in titanate oxides. For example, an insulating to metallic transition occurs at very small doping levels for $SrTi_{1-x}Nb_xO_3$ ($x < 0.0003$) [33], however at much higher doping levels for $BaTi_{1-x}Nb_xO_3$ ($x > 0.2$) [10]. In order to quantitatively evaluate the electrical properties of our doped PTNO films, resistivity versus temperature measurements are implemented. Figure 4 shows the electrical resistivity of PTNO as a function of the temperature. The resistivity becomes slightly smaller with increasing the temperature for $PbTi_{0.96}Nb_{0.04}O_3$, indicating an insulating behavior. There are at least two reasons why the resistivity stays at a large value with slightly doping. Firstly, the electrons liberated from the pentavalent Nb can be balanced by the holes provided by Pb vacancies. Therefore, far from lowering the resistivity, slight doping of Nb actually increases it [34]. Secondly, the extra electrons provided by Nb are not totally itinerant, instead they mainly locate around one Ti orbital. This will be further discussed later in the present paper based on our first-principles calculations. However, for the samples with more dopants, the resistivities of $PbTi_{0.94}Nb_{0.06}O_3$ and $PbTi_{0.92}Nb_{0.08}O_3$ decrease remarkably with increasing the temperature. More

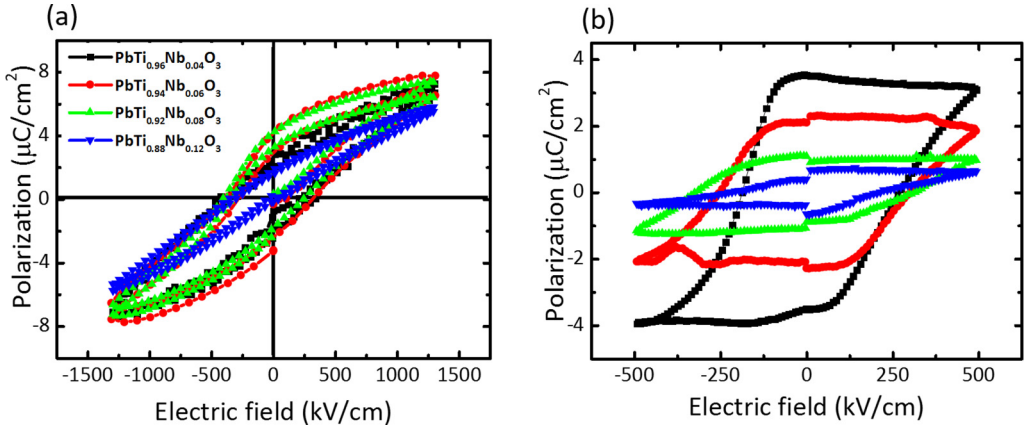

FIG. 3. (a) Ferroelectric *P-E* loops of the Au/PTNO/STNO heterostructures. (b) The *P-E* loops in the remnant polarization mode.

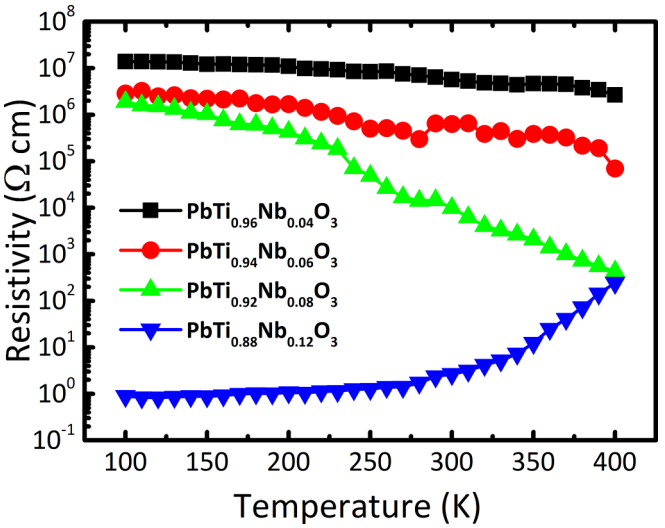

FIG. 4. Temperature dependence of electrical resistivity for PTNO films with Nb concentration varying from 0.04 to 0.12.

distinctively, the resistivity of $PbTi_{0.88}Nb_{0.12}O_3$ goes up with increasing the temperature. Therefore, we can conclude that, with the increase of Nb concentration from 0.04 to 0.12, the temperature-dependent transport behavior transforms from the insulating to the metallic.

For clarifying the underlying mechanism behind these phenomena, we carried out DFT calculations (detailed description for the calculation can be found in Sec. II). For simplicity, the 0.125 instead of 0.12 doping concentration is investigated by constructing a $2 \times 2 \times 2$ supercell of $PbTiO_3$ and substituting one Ti by Nb. Generally, doped electrons could localize and form an insulating phase, called the small polaron [35]. To study the conductive behavior, both delocalized and small polaron configurations need to be modeled. The delocalized solution can be achieved within a standard non-spin-polarized calculation. The small polaron configuration can be investigated by following the strategy proposed by Deskins *et al.* [36]. There are six inequivalent positions in the primitive cell of $Pb_8Ti_7NbO_{24}$ where the one excess electron could localize. All of the structures with different configurations are sufficiently relaxed. By taking the polar axis as the *c* axis, we found the most stable solution is that the wave function of the doped electron locates around one of the four Ti atoms nearest to the Nb atom in the *ab* plane, as shown in Fig. 5(a). The primitive cell deviates slightly from the tetragonal phase due to the Nb substitution. In the small polaron area, the TiO_6 octahedron is expanded due to the excess electron. Figure 5(a) also manifests that the spatial distribution of the electron-doped wave function decays from the localization center. The insulating behavior of our films with the doping level lower than 0.12 can be interpreted as the discretization of energy levels due to the weak wave-function overlap among the nearest doped electrons. The doped electron is not fully localized to open a band gap in this 0.125 doping case, being a metallic state with some localization, as shown in Fig. 5(b), which is consistent with our experimental results. In addition, the crystal structure obtained from DFT calculations also shows that the polar distortion is not distinctly suppressed by metallicity, as demonstrated in Fig. 5(c). The Ti^{4+}/Nb^{5+} cations have displacements from the center of the Pb8 cage around them, which is in line with the STEM images in Fig. 2. The survival of the noncentrosymmetric structure of $PbTi_{0.88}Nb_{0.12}O_3$ should be mainly because of the *ab*-plane distribution of the doped electron is not able to screen out the dipole in the *c* axis.

IV. SUMMARY

In summary, we experimentally realized the electron doping in $PbTiO_3$ by fabricating the PTNO films with various Nb concentrations. To verify that the piezoresponse signals stem from the local dipole in the unit cell, HAADF STEM images of the slightly doped $PbTi_{0.96}Nb_{0.04}O_3$ and the heavily doped $PbTi_{0.88}Nb_{0.12}O_3$ are used. We found that even the heavily doped $PbTi_{0.88}Nb_{0.12}O_3$ has a distinguishable domain structure

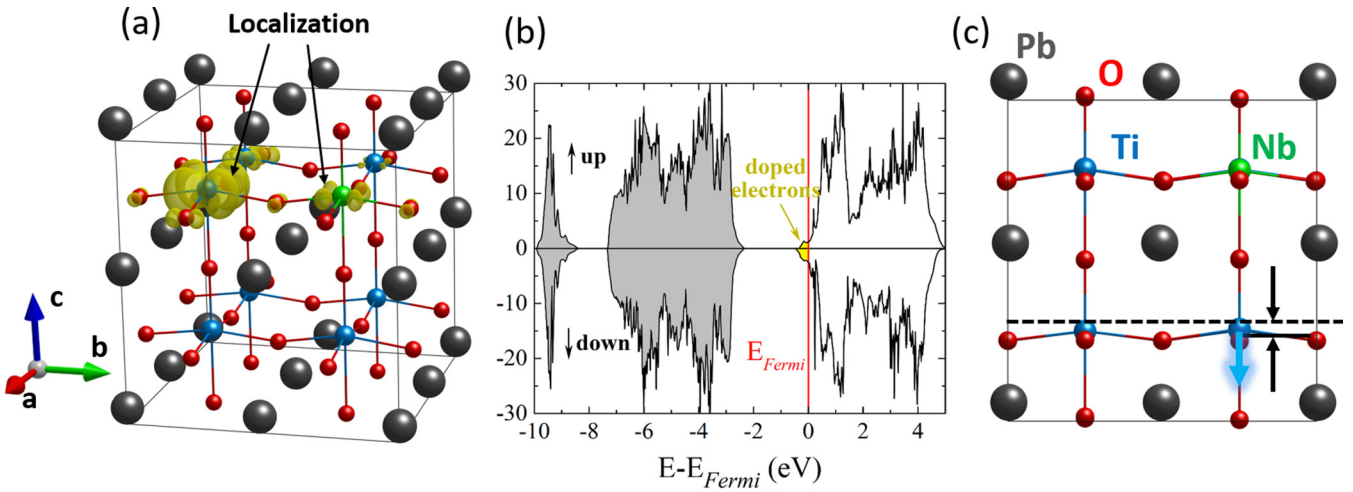

FIG. 5. (a) Isosurface (isovalue 0.04 eA^{-3}) of the doped electronic density for the most stable solution in the $Pb_8Ti_7NbO_{24}$ primitive cell. (b) Total density of states. The yellow area denotes the doped electronic density of states. (c) Side view of the $Pb_8Ti_7NbO_{24}$ primitive cell obtained from DFT. The black arrows mark the off-center displacement of the Ti atom, while the blue one marks the off-center direction of the Ti atom.

and an off-centering displacement of the Ti^{4+}/Nb^{5+} ions. In addition, the existence of a macroscopic remnant polarization measured by ferroelectric tester demonstrates that the polarization charges are not completely screened by the electrons doped in all of these films. The temperature-dependent resistivity measurements manifest that, with increasing Nb dopants, the PTNO films underwent a transition from an insulator to a metal. The itinerant electrons provided by Nb atoms present the metal-like behavior, whereas they cannot damage the polar distortions nor the individual dipole in each unit cell. The presented DFT results have revealed that the electrons doped in the 0.125 Nb-doping samples tend to form small polarons, but are not able to create a band gap. Thus, PTNO is proved to be in coexistence with the polar distortion and metallicity at room temperature, as a more promising candidate for ferroelectric metal, which was predicted decades ago but had few supporters up to now. It has been reported that polar metal presents unconventional optical responses, magnetoelectricity, and superconductivity properties [18–22]. We believe that this class of materials has potential applications on functional devices which desire high conductivity coexisting with the polarization fieldlike ferroelectric photovoltaic device. The present results should pave the way for doping some ferroelectrics for broadening this class of ferroelectric metals.

ACKNOWLEDGMENTS

The work was supported by the National Key Basic Research Program of China (Grants No. 2014CB921001, No. 2014CB921002, and No. 2013CB328706), the Key Research Program of Frontier Sciences of the Chinese Academy of Sciences (Grant No. QYZDJ-SSW-SLH020), the Strategic Priority Research Program (B) of the Chinese Academy of Sciences (Grant No. XDB07030200), and the National Natural Science Foundation of China (Grants No. 11674385, No. 11574365, No. 11474349, No. 51522212, No. 11404380, and No. 11721404).

[1] P. W. Anderson and E. I. Blount, Phys. Rev. Lett. **14**, 217 (1965).
[2] Y. G. Shi, Y. F. Guo, X. Wang, A. J. Princep, D. Khalyavin, P. Manuel, Y. Michiue, A. Sato, K. Tsuda, S. Yu, M. Arai, Y. Shirako, M. Akaogi, N. L. Wang, K. Yamaura, and A. T. Boothroyd, Nat. Mater. **12**, 1024 (2013).
[3] H. Sim and B. G. Kim, Phys. Rev. B **89**, 201107(R) (2014).
[4] G. Giovannetti and M. Capone, Phys. Rev. B **90**, 195113 (2014).
[5] H. M. Liu, Y. P. Du, Y. L. Xie, J. M. Liu, C.-G. Duan, and X. Wan, Phys. Rev. B **91**, 064104 (2015).
[6] I. Lo Vecchio, G. Giovannetti, M. Autore, P. Di Pietro, A. Perucchi, J. He, K. Yamaura, M. Capone, and S. Lupi, Phys. Rev. B **93**, 161113(R) (2016).
[7] F. Jin, A. Zhang, J. Ji, K. Liu, L. Wang, Y. Shi, Y. Tian, X. Ma, and Q. Zhang, Phys. Rev. B **93**, 064303 (2016).
[8] D. Puggioni and J. M. Rondinelli, Nat. Commun. **5**, 3432 (2014).
[9] A. Filippetti, V. Fiorentini, F. Ricci, P. Delugas, and J. Iniguez, Nat. Commun. **7**, 11211 (2016).
[10] L. Liu, H. Guo, H. Lü, S. Dai, B. Cheng, and Z. Chen, J. Appl. Phys. **97**, 054102 (2005).
[11] K. Page, T. Kolodiazhnyi, T. Proffen, A. K. Cheetham, and R. Seshadri, Phys. Rev. Lett. **101**, 205502 (2008).
[12] Y. Wang, X. Liu, J. D. Burton, S. S. Jaswal, and E. Y. Tsymbal, Phys. Rev. Lett. **109**, 247601 (2012).
[13] Y. Iwazaki, T. Suzuki, Y. Mizuno, and S. Tsuneyuki, Phys. Rev. B **86**, 214103 (2012).
[14] S. Raghavan, J. Y. Zhang, O. F. Shoron, and S. Stemmer, Phys. Rev. Lett. **117**, 037602 (2016).
[15] R. E. Cohen, Nature (London) **358**, 136 (1992).
[16] X. He and K.-j. Jin, Phys. Rev. B **94**, 224107 (2016).
[17] C. Ma, X. He, and K.-j. Jin, Phys. Rev. B **96**, 035140 (2017).
[18] V. P. Mineev and Y. Yoshioka, Phys. Rev. B **81**, 094525 (2010).
[19] V. M. Edelstein, Phys. Rev. B **83**, 113109 (2011).
[20] V. M. Edelstein, Phys. Rev. B **72**, 172501 (2005).
[21] E. Bauer, G. Rogl, X. Q. Chen, R. T. Khan, H. Michor, G. Hilscher, E. Royanian, K. Kumagai, D. Z. Li, Y. Y. Li, R. Podloucky, and P. Rogl, Phys. Rev. B **82**, 064511 (2010).
[22] E. Bauer, H. Kaldarar, R. Lackner, H. Michor, W. Steiner, E. W. Scheidt, A. Galatanu, F. Marabelli, T. Wazumi, K. Kumagai, and M. Feuerbacher, Phys. Rev. B **76**, 014528 (2007).
[23] E. Soergel, J. Phys. D: Appl. Phys. **44**, 464003 (2011).
[24] G. Kresse and D. Joubert, Phys. Rev. B **59**, 1758 (1999).
[25] G. Kresse and J. Furthmüller, Phys. Rev. B **54**, 11169 (1996).
[26] J. P. Perdew, K. Burke, and M. Ernzerhof, Phys. Rev. Lett. **77**, 3865 (1996).
[27] S. L. Dudarev, G. A. Botton, S. Y. Savrasov, C. J. Humphreys, and A. P. Sutton, Phys. Rev. B **57**, 1505 (1998).
[28] R. C. Ibrahim, T. Horiuchi, T. Shiosaki, and K. Matsushige, Jpn. J. Appl. Phys., Part 1 **37**, 4539 (1998).
[29] See Supplemental Material at http://link.aps.org/supplemental/10.1103/PhysRevB.96.165206 for details of the structure characterization and the out-of-plane piezoresponse amplitude images, which include Refs. [28], [37,38], [30], and [23], respectively.
[30] A. Torres-Pardo, A. Gloter, P. Zubko, N. Jecklin, C. Lichtensteiger, C. Colliex, J.-M. Triscone, and O. Stéphan, Phys. Rev. B **84**, 220102(R) (2011).
[31] Y. L. Tang, Y. L. Zhu, X. L. Ma, A. Y. Borisevich, A. N. Morozovska, E. A. Eliseev, W. Y. Wang, Y. J. Wang, Y. B. Xu, Z. D. Zhang, and S. J. Pennycook, Science **348**, 547 (2015).
[32] T. Iijima, H. Nafe, and F. Aldinger, Integr. Ferroelectr. **30**, 9 (2000).
[33] H. P. R. Frederikse, W. R. Thurber, and W. R. Hosler, Phys. Rev. **134**, A442 (1964).
[34] R. C. Ibrahim, T. Horiuchi, T. Shiosaki, and K. Matsushige, Jpn. J. Appl. Phys. Part 1 **37**, 6060 (1998).
[35] X. F. Hao, Z. M. Wang, M. Schmid, U. Diebold, and C. Franchini, Phys. Rev. B **91**, 085204 (2015).
[36] N. A. Deskins, R. Rousseau, and M. Dupuis, J. Phys. Chem. C **115**, 7562 (2011).
[37] R. Mastelaro, P. P. Neves, A. Michalowicz, and J. A. Eiras, J. Phys.: Condens. Matter **19**, 226212 (2007).
[38] E. Arenholz, G. van der Laan, A. Fraile-Rodríguez, P. Yu, Q. He, and R. Ramesh, Phys. Rev. B **82**, 140103 (2010).